A Comparative Analysis of HIGA loaded i-SMR core Model Using DeCART/MASTER and Serpent2

Woo Jin Lee, Seungnam Lee and Ser Gi Hong*
Departments of Nuclear Engineering, Hanyang University, 222, Wangsimni-ro, Seongdong-gu, Seoul, 04761, Republic of Korea
**Corresponding author: hongsergi@hanyang.ac.kr*

Keywords : i-SMR, HIGA, Gadolinia, Serpent 2, DeCART/MASTER

1. Introduction

Small Modular Reactors (SMRs) are receiving significant attention as next-generation reactor technology due to their enhanced economic feasibility through modularization and passive safety features. i-SMR is currently under development in South Korea [1]. However, compared with the conventional large reactors, SMRs present unique characteristics such as higher neutron leakage, innovative fuel and burnable absorber designs. Therefore, the traditional two-step method using nodal methods based on assembly-wise homogenization with lattice code may encounter difficulties in accurately modeling these unique design characteristics.

Specifically, the i-SMR incorporates innovative concepts such as boron-free operation, relying solely on control rods and innovative burnable absorbers (BA) for reactivity control. The use of these innovative concepts leads to the considerable changes of the core performance parameters such as power distribution and temperature reactivity coefficients from the commercial PWRs. Therefore, the core physics parameters are needed to be thoroughly validated from comparisons with high fidelity calculations to get license from the regulatory body.

The objective of this paper is to evaluate the accuracy of the two-step core design and analysis code system DeCART2D1.1[2]/MASTER4.0[3] for an i-SMR core model employing an innovative BA concept known as Highly Intensive and Discrete Gadolinia Burnable Absorber (HIGA) rods [4]. The HIGA is a discrete-type BA composed of a sintered mixture containing 10–20 mol% Gd_2O_3, with the remainder being Al_2O_3. Accurate modeling of i-SMR core employing HIGA requires accurate representation of the rapidly changing microscopic neutron capture cross sections of Gd as burnup, as well as the high neutron leakage characteristic of SMRs.

In this work, the validation is performed by following two steps: 1) Validation of fuel assembly (FA) depletion calculations and 2) Validation of core depletion calculations through the comparison of the analysis results with those obtained from the high-fidelity Monte Carlo (MC) reference code SERPENT 2 [5], for the 1st cycle of i-SMR core adopted from reference paper [4].

2. Calculation Conditions and Computer Codes for Modeling

2.1 2D Fuel Assemblies

Table I summarizes the specifications of the FAs for the 1st cycle i-SMR core adopted from the reference paper [4] for modeling purposes. The core consists of various FA configurations optimized according to the characteristics of HIGA rods and Integral Gadolinia (IGD) BA rods. Specifically, eight FA types have been designed, each containing 4 to 12 IGD rods (1–8 wt.% Gd_2O_3) and 16 HIGA rods (10–18 mol.% Gd_2O_3), while maintaining a constant ^{235}U enrichment of 4 wt.% for all fuel rods.

Fig. 1 shows an example of 1/8 A8 type FA configuration, consisting of a 17×17 lattice arrangement with 24 guide tubes, one instrumentation tube, 12 IGD rods, and 16 HIGA rods.

Table I: Fuel assembly specifications for the 1st cycle in the i-SMR core [4]

	Fuel rod	HIGA rod	IGD rod			
			1st		2nd	
	^{235}U (wt.%)	Gd_2O_3 (mol.%)	^{235}U (wt.%)	Gd_2O_3 (wt.%)	^{235}U (wt.%)	Gd_2O_3 (wt.%)
A1	4.0	10	-	-	-	-
A2	4.0	10	3.50	4	-	-
A3	4.0	12	3.50	4	-	-
A4	4.0	14	3.50	4	2.50	8
A5	4.0	15	3.50	4	2.50	8
A6	4.0	16	3.50	4	2.50	8
A7	4.0	18	3.95	1	2.50	8
A8	4.0	18	3.75	2	2.50	8

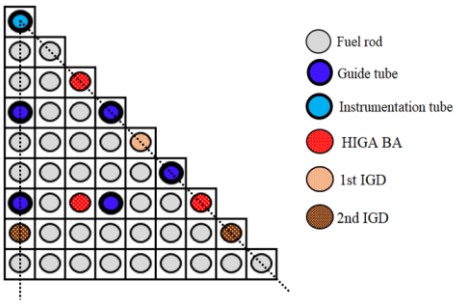

Fig. 1. Octant configuration of A8 type FAs

Table II summarizes the calculation conditions used in the DeCART2D code for generating assembly-wise homogenized group constant (HGC) to be utilized in the core calculations using MASTER. For validation of the fuel depletion calculation using DeCART2D, the Serpent 2 was also employed to perform 2D FA

modeling. Both sets of calculation conditions are listed in Table II for comparison.

Both the codes employed the same temperature conditions and the cross-section data derived from ENDF/B-VII.1. Specifically, DeCART2D utilized the 47-group neutron and 18-group gamma library (DML-E71N047G018-PV01-cr08.BIN [2]) based on ENDF/B-VII.1. In addition, Serpent 2 employed thermal scattering libraries (lwtr for hydrogen in water, and thermal scattering for O and U in UO_2). In the Serpent 2 depletion calculation, the fuel pellet depletion was modeled with three radial zones, whereas the burnable absorber (BA) pellet was modeled with eight radial zones to accurately capture self-shielding effects.

The Serpent 2 code employed 1,000,000 neutron histories per cycle (100 active cycles and 50 inactive cycles), resulting in a k_{inf} standard deviation of approximately 6–7 pcm. The DeCART2D employed the Method of Characteristics (MOC) with a ray spacing of 0.01 cm, 16 azimuthal angles per octant, and 4 polar angles. For depletion calculations, Serpent 2 utilized the 16th-order CRAM solver, while DeCART2D used the Krylov subspace method. The number of depletion steps was identical in both codes to ensure a consistent comparison.

Table II: Calculation conditions for fuel assembly modeling in Serpent and DeCART2D

Category	Serpent 2	DeCART 2D
Temperature (K)	UO_2 pellet: 900K Cladding: 600K Moderator: 580K	
Number of depletion Zones	UO_2 pellet: 3 BP pellet: 8	
XS library	ENDF/B-VII.1	
Neutron Histories (MC) / Ray tracing (MOC)	1,000,000 per Cycle 100 Active Cycles 50 Inactive Cycle	Ray Spacing: 0.01 cm Azimuthal Angle: 16 Polar Anlges: 4
Depletion solver	CRAM 16th order	Krylov subspace
Depletion step size (MWd/kgHM)	**0.1** from 0 to 1 **0.5** until Gd depletion, **1** thereafter	

2.2 Reflector modeling in DeCART2D

Due to the smaller size of i-SMRs compared to large reactors, neutron leakage effects become more significant. Additionally, to mitigate axial power skewness towards the bottom region, the core design employs an upper axial cutback, resulting in an axial power shift towards the upper region. Therefore, accurate preparation of radial and axial reflector cross-section (XS) is essential.

Fig. 2 shows the radial and axial reflector models to generate reflector XS for subsequent core nodal calculations in MASTER.

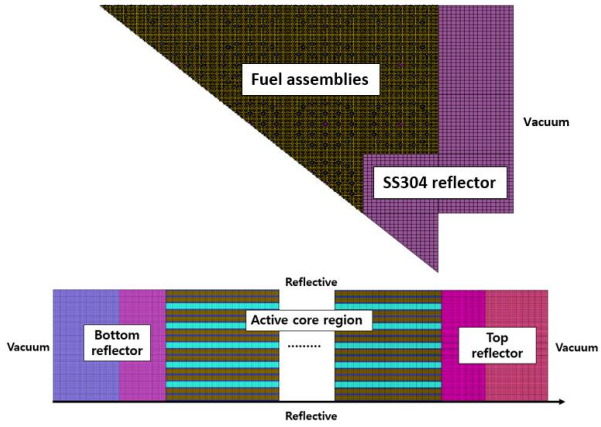

Fig. 2. Configuration of radial and axial reflector designs by DeCART2D code

The radial reflector XS was prepared through two-dimensional heterogeneous neutron transport calculations performed using the DeCART2D code for an octant core model. In the radial reflector modeling, the reflector region was represented by SS304 reflector nodes with dimensions of 21.5 cm × 21.5 cm.

Axial reflector XS were also generated using DeCART2D neutron transport calculations. For axial reflector modeling, a simplified 1D core model consisting of a vertically arranged assembly was employed instead of the conventional two-node approach [6].

The active core region in this model consists repetitive arrangements of fuel rod and guide tubes. Reflective boundary conditions were applied at both the top and bottom boundaries of the horizontal model. Top and bottom reflectors were modeled as homogenized mixtures of stainless steel and moderator materials, each with a node size equal to the FA pitch (21.5 cm). A vacuum boundary condition was applied on the left side of the bottom reflector and the right side of the top reflector.

Once the axial and radial reflector XSs are prepared, the reflector HGC files are processed using PROMARX [7] to generate effective radial and axial reflector XS data, which are subsequently utilized in MASTER.

2.3 3D Reactor Core

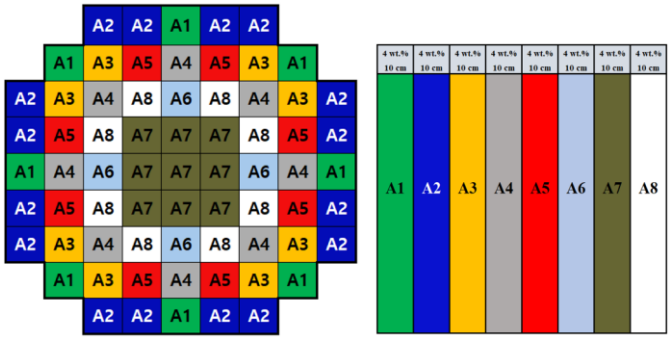

Fig. 3. Radial and axial configuration of i-SMR core [4]

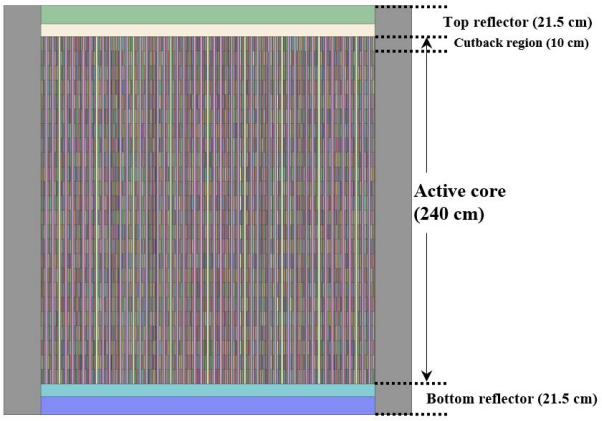

Fig. 4. Axial configuration of i-SMR core model in Serpent 2

Fig. 3 illustrates the radial and axial configurations of the reference i-SMR core. The reference core loading pattern places FA with higher excess reactivity at the peripheral regions to flatten the radial power distribution and includes an upper 10 cm region designed to mitigate axial power skewness.

A modified version of the reference core configuration was employed in this study, because the axial reflector node size was not explicitly provided in the reference. Therefore, it was assumed that both MASTER and Serpent 2 adopt the identical axial discretizations, dividing the active core length of 240 cm into 24 axial nodes and setting the axial reflector node size to 21.5 cm.

Fig. 4 illustrates the corresponding Serpent 3D core model. To ensure statistical accuracy, the Serpent simulation utilized 15,000,000 neutron histories per cycle (100 active cycles, 50 inactive cycles), resulting in a k_{eff} standard deviation of approximately 3–4 pcm.

Fixed fuel and moderator temperatures (900 K and 580 K, respectively) were applied for consistency, and thermal-hydraulic feedback was deactivated the MASTER because our Serpent 2 calculations do not consider the thermal-hydraulic feedback.

3. Numerical Results and Comparison

3.1. 2D Fuel Assemblies

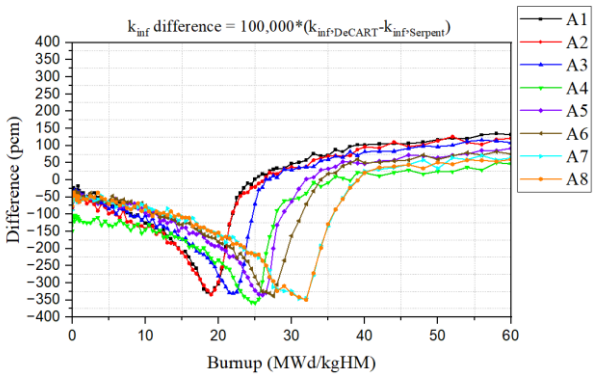

Fig. 5. Comparison of k_{inf} difference between DeCART and Serpent for various FA types

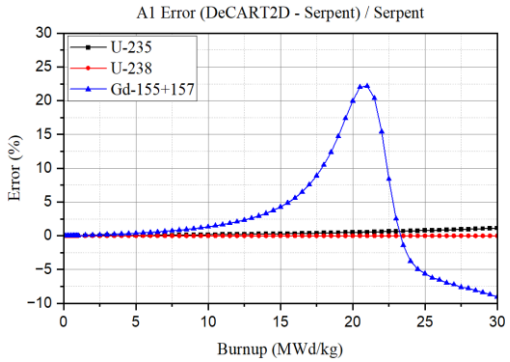

Fig. 6. Comparison of Uranium and Gadolinium isotopes concentrations in A1 FA between DeCART and Serpent

Fig. 5 shows the comparison of the k_{inf} differences between DeCART and Serpent for various FA types as a function of burnup.

In general, the differences between the two codes remain within ±100 pcm over most burnup ranges. However, relatively larger differences of up to approximately ±350 pcm are observed at the intermediate burnup levels (20–35 MWd/kgHM), coinciding with the nearly complete depletion of Gd isotopes in BAs.

Figure 6 supplements this observation by showing isotopic concentration errors for ^{235,238}U and ^{155,157}Gd in the A1 type assembly. Because the Gd isotopic concentrations calculated by DeCART2D show significant positive errors during this burnup interval, the resulting k_{inf} differences become correspondingly negative and notably large.

Although the same burnup step sizes were applied in both codes as shown in Table II, the error may originate from differences in depletion solvers, as well as differences in the XS libraries used to model Gds.

Given that Serpent 2 MC calculations are typically regarded as a high-fidelity reference, these results highlight the need for an improved XS library in DeCART2D capable of accurately capturing the rapid changes associated with Gd depletion.

3.2. 3D Reactor Core

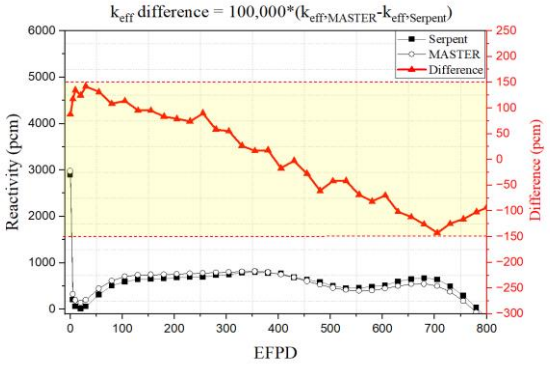

Fig. 7. Comparison of 3D core reactivity evolutions and k_{eff} difference between MASTER and Serpent 2

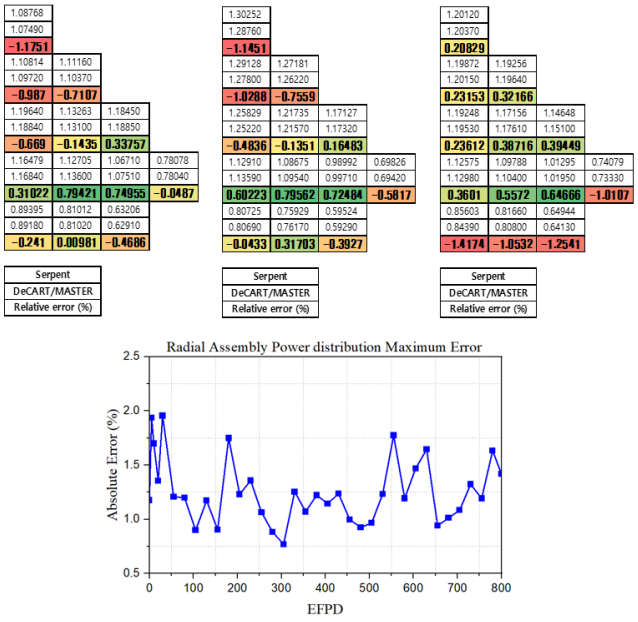

Fig. 8. Comparison of Radial Assembly Power Distribution and Maximum Error between MASTER and Serpent 2

Figure 7 compares the core reactivity calculated by MASTER and Serpent as a function of Effective Full Power Days (EFPD). The MASTER results show excellent agreement with Serpent, with reactivity differences generally within ±150 pcm throughout the cycle. Slightly large differences observed at the beginning of the cycle (BOC) are mainly due to the initial depletion of IGD BAs. Similar trends—a negative bias up to about 20 MWd/kgHM (around 700 EFPDs), followed by a gradual positive shift—were noted in the FA-level calculations (Fig. 5), indicating that difference arising at the FA level, particularly related to Gd depletion, directly propagate into full-core calculations. Nevertheless, overall agreement at the core level remains good, demonstrating the adequacy of the current modeling approach.

Figure 8 compares the radial assembly-wise power distributions calculated by MASTER and Serpent 2 at representative burnup points (BOC, MOC, and EOC). The relative power differences between the two codes remain within ±2% for all FAs. The maximum absolute error as a function of EFPD is also shown, illustrating consistently good agreement.

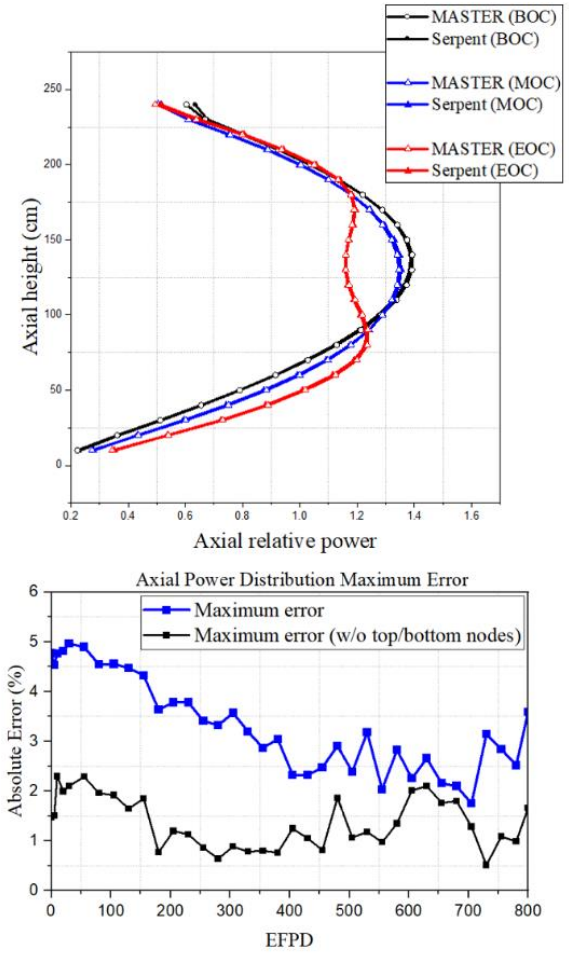

Fig. 9. Comparison of Axial Power Distributions and Maximum Errors between MASTER and Serpent

Figure 9 compares the axial power distributions calculated by MASTER and Serpent 2 at BOC, MOC, and EOC. Overall, the results from MASTER show excellent agreement with Serpent 2, with axial power distribution errors consistently below approximately 2% throughout the cycle, excluding near the axial reflector boundary nodes.

Larger differences (up to ~5%) observed near the reflector boundaries, particularly in the upper core region, are primarily attributed to the top-skewed power distribution resulted from the upper cutback design in the boron-free core.

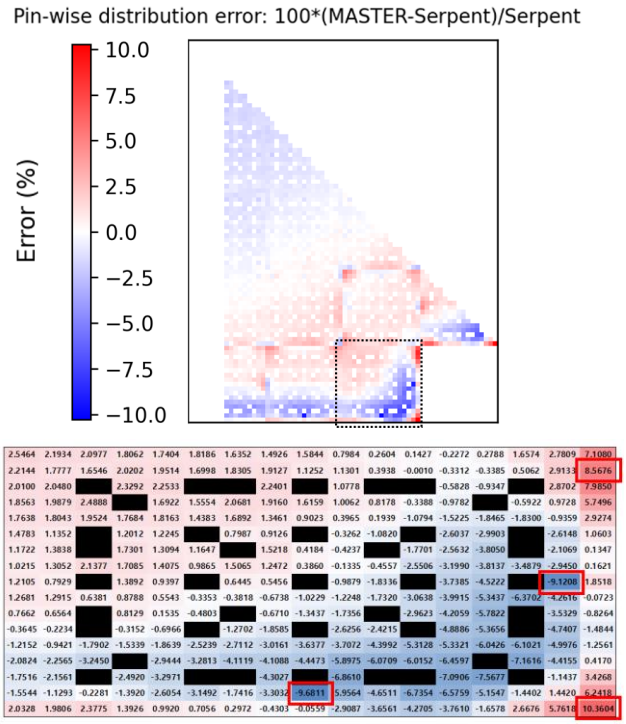

Fig. 10. Pin power distribution error and detailed error in selected regions

Figure 10 presents the pin-wise power distribution error expressed as a percentage relative to Serpent. The top portion is a heatmap indicating positive (red) and negative (blue) deviations, while the bottom figure zooms in on the assembly region where the maximum pin errors occur (highlighted by the dashed box). Notably, four pins designated by red line box stand out with higher differences.

The reflector-adjacent pin in the lower-right corner shows a maximum error of 10.36%, another pin in the upper-right corner has an 8.56% difference, and two IGD pins exhibit errors of 9.12% and 9.68%.

These larger deviations typically appear at the periphery or near reflectors, where steep flux gradients and localized burnable absorber depletion are more pronounced. In contrast, the errors for pins except for the periphery region remain below 5%.

Table III: Comparison of integral control bank worth in the All-Rods-In state

Control Bank type	Serpent (pcm)	MASTER (pcm)	Difference (pcm)
R1	2967	3016	49
R2	1196	1149	-46
R3	1564	1575	11
R4	1564	1517	47
S1	410	374	35
S2	1273	1217	45
S3	2044	2054	10
S4	2647	2737	89
S5	1652	1722	69
S6	801	813	11

Finally, Table III compares the integral control bank worth values calculated by Serpent 2 and MASTER when each control bank is fully inserted individually Overall, the differences remain within 90 pcm, indicating that MASTER closely follows the Serpent results in capturing the global reactivity effect of control rod insertion. However, further investigation is required to determine the magnitude of differences in local effects during control rod insertion.

4. Conclusions

In this work, a comprehensive comparison was performed between the two-step core analysis code system of DeCART2D/MASTER and the high-fidelity MC code Serpent 2 for an innovative i-SMR core model featuring advanced BA designs (HIGA and IGD rods). The main findings are summarized as follows:

1) Global Core Performance:

3D core calculations demonstrate that MASTER closely follows the global behavior calculated by Serpent 2. The overall reactivity differences remain within ±150 pcm, and the FA-wise radial power distributions agree within ±2% for most assemblies. Furthermore, the comparisons of control rod worth indicate that MASTER effectively captures the global reactivity effects, thereby validating the nodal diffusion approach at the system level.

2) Gd Depletion:

Discrepancies become more significant during the rapid depletion of Gd isotopes in HIGA. This finding shows the need for an improved cross-section library and treatment method considering resonance self-shielding effect and in DeCART2D to more accurately capture the rapid changes associated with Gd depletion in HIGA.

3) Local Effects:

While the global core parameters are well captured, local differences—such as those observed in the pin power distribution, particularly in peripheral and reflector-adjacent regions—indicate that further analysis is needed. To accurately capture these local effects, a pin-by-pin core analysis approach may be necessary.

Acknowledgment

We are very grateful to Prof. Joo Il Yoon at KINGS for his kind and valuable discussions on the results.
This work is financially supported by the Korea Institute of Energy Technology Evaluation and Planning (KETEP) grant funded by the Ministry of Trade, Industry and Energy (MOTIE) of Republic of Korea (No. RS-2025-00398867) and by the Nuclear Safety Research Program through the Regulatory Research Management Agency for SMRS (RMAS) and the Nuclear Safety and Security Commission (NSSC) of the Republic of Korea (No. RS-2025-00509678).

REFERENCES

[1] Kang, H. O., Lee, B. J., & Lim, S. G. (2024). Light water SMR development status in Korea. Nuclear Engineering and Design, 419, 112966.
[2] J. Y. Cho, et al., "DeCART2D v1.1 User's Manual," KAERI/UM-40/2016, 2016.
[3] J. Y. Cho, et al., "MASTER v4.0 User's Manual," KAERI/UM-41/2016, 2016.
[4] Kim, J. S., Jung, T. S., & Yoon, J. (2024). Reactor core design with practical gadolinia burnable absorbers for soluble boron-free operation in the innovative SMR. Nuclear Engineering and Technology, 56(8), 3144-3154.
[5] Leppänen, J., et al., "The Serpent Monte Carlo code:Status, development and applications in 2013", Annals of Nuclear Energy, Vol.82, 142-150, 2015
[6] Shim, C. B., Lee, K., & Cho, J. Y. (2016, October). Improvement of axial reflector cross section generation model for PWR core analysis. In Transactions of the Korean Nuclear Society Autumn Meeting, Gyeongju, Korea.
[7] J. S. Song, et al., "PROLOG1.1 User's Manual," KAERI/UM-4/99, 1999.